Colloids and Surfaces B: Biointerfaces 222 (2023) 113068

Contents lists available at ScienceDirect

Colloids and Surfaces B: Biointerfaces

journal homepage: www.elsevier.com/locate/colsurfb

Surface-facilitated formation of polydopamine and its implications in melanogenesis

Chan Yeon Kim [a,1], Yoonyoung Kim [a,1], Min Young Lee [a], Seong Ah Jo [a], Seung-Woo Kim [b], Sung Min Kang [c], Young-Kwan Kim [b,*], Kyungtae Kang [a,*]

[a] Department of Applied Chemistry, Kyung Hee University, 1732 Deogyoung-daero, Yongin, Gyeonggi 17104, South Korea
[b] Department of Chemistry, Dongguk University, 30 Pildong-ro, Jung-gu, Seoul 04620, South Korea
[c] Department of Chemistry, Chungbuk National University, Cheongju, Chungbuk 28644, South Korea

ARTICLE INFO

Keywords:
Surface-driven polymerization
Polydopamine
Peptides
Amyloids
Melanogenesis

ABSTRACT

This manuscript examines influences of differently functionalized surfaces on the formation of solution-dispersed polydopamine (pDA). Glass vials functionalized with different functional groups provided a set of conditions with which the relationship between the area of active surface and the rate of pDA formation could be systematically studied. The results suggest that charged and polar surfaces accelerate pDA formation in solution, with the effect of -NH_2 surfaces being exceptionally strong. In the vials, pDA formed as both forms of dispersions in solution and films at solid-liquid interface. Further analyses confirmed that both forms of pDA formed with -NH_2 surfaces were chemically similar to conventional pDA synthesized without help of functional surfaces. Among short peptide-based amyloid fibers with defined surface functional groups, and those displaying lysines (-NH_2) greatly accelerated the formation of pDA, consistent with the results of -NH_2-functionalized vials. The results suggest that pDA formation may be facilitated by surface functional groups of solid-liquid interfaces, and have implications for the overlooked roles of amyloid fibers in biological melanogenesis.

1. Introduction

Melanins—a family of natural pigments synthesized from *L*-dopa—have consistently attracted research interest since their discovery, because of their functional versatility and wide occurrence in many organisms [1]. Depending on the molecular composition, melanins in humans are categorized as eumelanin (synthesized primarily from *L*-dopa), pheomelanin (including *L*-cysteine as an additive), and neuromelanin (molecularly similar to eumelanin, but contain more proteins and lipids) [2]. Melanins also exist in other organisms carrying out diverse functions, such as coloration of bird feathers [3], functions of cephalopod ink [4], cuticle sclerotization [5], pathogenic activities of fungi [6,7], and self-protection of bacteria[8]. Inspired by various superior materials properties of melanins, efforts to chemically synthesize artificial versions of melanins—mostly eumelanin—have been increasingly attempted. Among others, polydopamine (pDA), which is synthesized by oxidation of dopamine in a basic buffer solution, is being utilized in various forms (e.g., films, particles, and fibers) for an enormously broad range of applications, including functional coatings [9–11], photothermal therapy [12–15], energy materials [16–20], and other functional nanostructures [21–25]. Despite these numerous efforts, it is still difficult to fully recapitulate diverse functions of natural melanins, because of the complexity that resides in their molecular composition and structure.

Natural eumelanin and its chemically synthesized equivalents are roughly similar but are different in a few aspects, such as detailed morphological features, light absorption, radical scavenging efficiency, and water sorption [26,27]. Biological melanogenesis relies on a cascade of enzymatic reactions, whereas chemical synthesis of melanins is conducted by simple oxidation of a dopamine derivative. This causes differences in chemical composition between them, among which the most remarkable is the relative composition of 5,6-dihydroxyindole (DHI) and 5,6-dihydroxyindole carboxylic acid (DHICA) [28–30]. A relatively underappreciated—but critical—aspect of biological melanogenesis is the involvement of a proteinaceous scaffold that exhibits an amyloid structure. In a melanosome, a melanosomal protein, Pmel17, is

* Corresponding authors.
E-mail addresses: kimyk@dongguk.edu (Y.-K. Kim), kkang@khu.ac.kr (K. Kang).
[1] These authors contributed equally to this manuscript.

https://doi.org/10.1016/j.colsurfb.2022.113068
Received 9 October 2022; Received in revised form 25 November 2022; Accepted 30 November 2022
Available online 1 December 2022

expressed intraluminally and spontaneously assembled to form amyloid fibers [31–33]. The role of Pmel17 fibers in melanogenesis has long been considered somewhat less significant; previous related works suggested that Pmel17 fibers primarily act as a matrix for sequestering potentially harmful intermediates that appear during melanogenesis [34–36]. The functions of Pmel17 fibers, however, may be more diverse and crucial than expected; they survived the evolutionary process from bacteria to humans. Throughout a series of previous works, we have recently shown that amyloid fibers (of Pmel17 and other proteins) have diverse functions regarding the formation process and properties of pDA, including catalytic acceleration of its formation and regulation of its morphology, water-dispersibility, and even spin concentration [37–39]. The molecular principles of such multifaceted functions are, however, far from understood, albeit its potential relevance to other supramolecular functionalities prevalent in nature.

To this end, we started with an assumption that the spatial orientation of functional groups is the key in the observed functions of amyloid fibers. Amyloid fibers tend to present polar (charged, in particular) residues on their surface, while burying nonpolar residues inside [40]. Periodic and proximal molecular configuration of polar residues often leads to unexpected catalytic activities, as in some cases of enzymes or supramolecular materials. We used glass vials as a simplified model solid-liquid interface (i.e., surface) whose molecular structure is carefully controlled. Facilitating influences of molecularly derivatized surfaces for pDA formation were assessed, and their chemical properties on surface and in solution were comparatively investigated. To verify our initial assumption, we also synthesized short peptide-based amyloid fibers designed to display certain polar side chains on their surface. This study reveals that solution-phase pDA formation can be accelerated by surface-oriented functional groups, which has implications in the role of Pmel17 fibers in biological melanogenesis. It also emphasizes the importance of local molecular orientation in supramolecular catalysis.

2. Materials and methods

2.1. Materials

The following chemicals, phosphate-buffered saline (PBS; pH 7.4) and dopamine hydrochloride were purchased from Thermo Fisher Scientific. Rink Amide MBHA resin HL and *N*,*N*,*N*′,*N*′-Tetramethyl-*O*-(1*H*-benzotriazol-1-yl)uranium hexafluorophosphate (HBTU, 98%) were purchased from Alfa Aesar (USA). 1 M Tris-HCl, pH 8.5 was purchased from Biosesang (South Korea). Fmoc-protected amino acids and *N*,*N*-diisopropylethylamine (DIPEA, 99%) were purchased from TCI (Japan). Acetic anhydride (99.5%) was purchased from Sigma-Aldrich (USA). *N*, *N*-dimethylformamide (DMF, 99.0%) for peptide synthesis (99.8%) was purchased from Acros Organics (USA). Trifluoroacetic acid (99.0%), methyl alcohol (HPLC grade), acetonitrile (HPLC grade), water (HPLC grade), dichloromethane (99.5%) and ethyl ether (99.5%) were purchased from Samchun (South Korea). All reagents were used without any further purification. Microscope slides (DU. 2355031) were purchased from Daihan Scientific (South Korea). 30 mL-vials (SCV-30) were purchased from Dawonscience (South Korea). A C18 column was purchased from Thermo Fisher Scientific (USA).

2.2. Synthesis and purification of peptides

[Ac-IHIHIYI-NH_2] and [Ac-IKIKIYI-NH_2] sequences were synthesized by Fmoc-based solid-phase synthesis, using Rink-amide MBHA resin at room temperature. Fmoc groups were removed by repeated reactions (10 min) with a 20% piperidine solution. Amide coupling was conducted by mixing a protected amino acid, HBTU, and DIPEA in DMF. The coupling reaction took 2 h at room temperature. After all the seven amino acids were coupled, the *N*-terminal of the peptide was acetylated with acetic anhydride and pyridine in DMF. Cleavage and side chain deprotection were accomplished by treating the cleavage cocktail for 2 h at room temperature after acetylation. The cleavage cocktail was prepared by mixing trifluoroacetic acid, triisopropylsilane, and DCM (95:2.5:2.5, v/v). After the synthesis was complete, crude products were purified via reverse-phase high-performance liquid chromatography with a C18 column. Peptides were lyophilized after purification.

2.3. Synthesis of amyloid fibers and subsequent pDA formation

Amyloid fibers were prepared by dissolving purified peptides in 25 mM Tris-HCl buffer (pH 8.5) and incubated at 37 °C, 200 rpm for 1 h to make peptides self-assemble. After incubation, the solution was centrifuged (15,000 rpm, 15 min) and the supernatant was discarded. The concentration of amyloid fibers was indirectly calculated by measuring the absorbance at 280 nm of the supernatant (i.e., the concentration of the remaining peptide monomers) after incubation. The precipitated amyloid fibers were redispersed in a PBS solution (pH 7.4) and mixed with dopamine in a cuvette. The final concentrations of amyloid fibers and dopamine were 150 μM. Cuvettes were placed in an orbital shaker (250 rpm) at room temperature.

2.4. UV–visible (UV–VIS) spectroscopy

The UV–VIS absorbance spectra of solutions containing pDA were taken for a wavelength range of 300–800 nm by using Lambda 465 (PerkinElmer, Inc., USA). The absorbance spectra of pDA synthesized with amyloid fibers were taken for a wavelength range of 250–800 nm. Before measuring each absorbance, cuvettes were vortexed and sonicated for 10 s.

2.5. Atomic force microscopy (AFM) analysis

AFM imaging of substrates was performed on an atomic force microscope (XE-150, Park systems, South Korea). An NCHR-50 (NanoWorld, Switzerland) AFM cantilever (typical resonant frequency of 320 kHz and force constant of 42 N m^{-1}) was employed in the non-contact mode for the determination of topographic profiles. The root-mean-square roughness (Rq) was determined over a 5 × 5 μm^2 area.

2.6. Field-emission scanning electron microscopy (FE-SEM)

A solution containing pDA was centrifuged at 13,000 rpm for 10 min, and the pellet was rinsed with DI water. The resultant pDA aggregates were re-dispersed in 2 mL of DI water and deposited on a Si wafer for drying in an oven (80 °C). The morphology of pDA was analyzed with FE-SEM S-4800 (Hitachi, Japan).

2.7. Laser desorption/ionization time-of-flight mass spectrometry (LDI-TOF-MS)

LDI-TOF-MS analysis was performed using IDSys (ASTA, Korea) with a Nb:YAG laser having a wavelength of 343 nm, a pulse rate of 1 kHz, and 50 μm in spot diameter at a target plate. The accelerating voltage was 18 kV in positive ionization mode. All mass spectra were obtained by averaging 100 laser shots. For LDI-TOF-MS analysis, 1 μL of reaction mixtures of pDA was spotted on a stainless-steel target plate, dried under ambient condition, and subjected to LDI-TOF-MS analysis, respectively.

2.8. Ellipsometry

The thickness and refractive index of the coatings were determined with an alpha-SE spectroscopic ellipsometer (J. A. Woollam) in the wavelength range of 390–900 nm at an incident angle of 70°. The data were fitted to a Cauchy model using the CompleteEASE software. Refractive index $n(\lambda) = 1.45 + 0.01/\lambda^2$).

2.9. Water contact angle measurement

Water contact angles were measured using a phoenix 300 (SEO co., Ltd, Korea). 10 μL of deionization water was dropped on each sample and the static contact angle was measured with ImageXP software.

3. Results

To quantitatively assess the influences of a polar surface on pDA formation, we first designed a minimalistic experiment using a glass vial. By injecting different volumes of an aqueous solution of dopamine (2 mg/mL in DI water) into O_2 plasma-treated glass vials, solutions having different ratios of solid-liquid interface area (i.e., active surface area) and volume (A/V) could be conveniently generated (Fig. 1a), which provide a set of reaction conditions with which influences of the area of the surface can be systematically assessed. Prolonged incubation of dopamine solutions exhibited a linearly decreasing trend in the darkness of solution (which reflects the amount of pDA dispersed in the solution) in respect to the volume of the injected solution (Fig. 1b), indicating a proportional relationship between the area of polar surface and the amount of pDA dispersed in solution. UV–VIS spectra collected from each solution, which commonly exhibited a gradual increase of broad and monotonic light absorption (a representative feature of pDA derivatives), showed such a trend more clearly (Figs. 1c and S1). Plotting light absorption at 450 nm (A_{450}; as a quantitative metric for the amount of solution-phase pDA) against the calculated A/V ratios of different solutions revealed their linear correlation (Fig. 1d). To rule out the potential influence of the accessible amount

of O_2 in each solution, we conducted the same experiment with vials capped with a punched top and found that punched tops did not cause significant changes in the amount of pDA (Fig. S2). The results suggest that the pDA formation in deionized water (DI water) is quantitatively correlated to the area of polar (in this particular case, negatively charged) surface.

As the O_2 plasma-treated glass surface is competent with the well-known silane-based covalent modifications, we next sought to compare a set of surfaces with different terminal functional groups for their influences on solution-dispersed pDA formation. The set of functional groups was chosen to include non-polar, polar, charged, and nucleophilic moieties (Fig. S3 and S4). Aqueous solutions of dopamine (4 mL, 2 mg/mL) were incubated in vials functionalized with different functional groups. As shown in Fig. 2a and b, the set of functional groups could be grouped into three categories in respect to their influence on pDA formation: (i) -CH_3, -OH, -SH, and -COOH surfaces promoted pDA formation to the extent similar to the bare (O_2 plasma-treated) vial. (ii) Only -NH_2 surface promoted pDA formation better in respect to the bare vial, while (iii) the most hydrophobic -CF_3 surface did adversely so (Fig. S5). The -NH_2 surfaces showed the same trend between A/V ratio and the rate of pDA formation, as the case of the bare vial (Fig. 2c). The results suggest that surfaces with a broad range of terminal functional groups are capable of moderately promoting pDA formation, with an exception of the very hydrophobic -CF_3 surface. The molecular origins of such global surface activity of many functional groups are unclear, but are presumably related to the multimodal repertoires of a catechol group for interacting with various other functional surfaces, which form a basis for material-independent formation of pDA coating [41]. The highest activity of the -NH_2 surface was expectable from previous reports [39], and strongly suggests that amine groups play roles as a nucleophile or a positive charge, which covalently (via imine formation) or non-covalently (via cation-π interactions) recruits dopamine and its oxidative intermediates near the surfaces, respectively. Such an influence of the -NH_2 surface remained consistent over a broad range of pH (7–11)

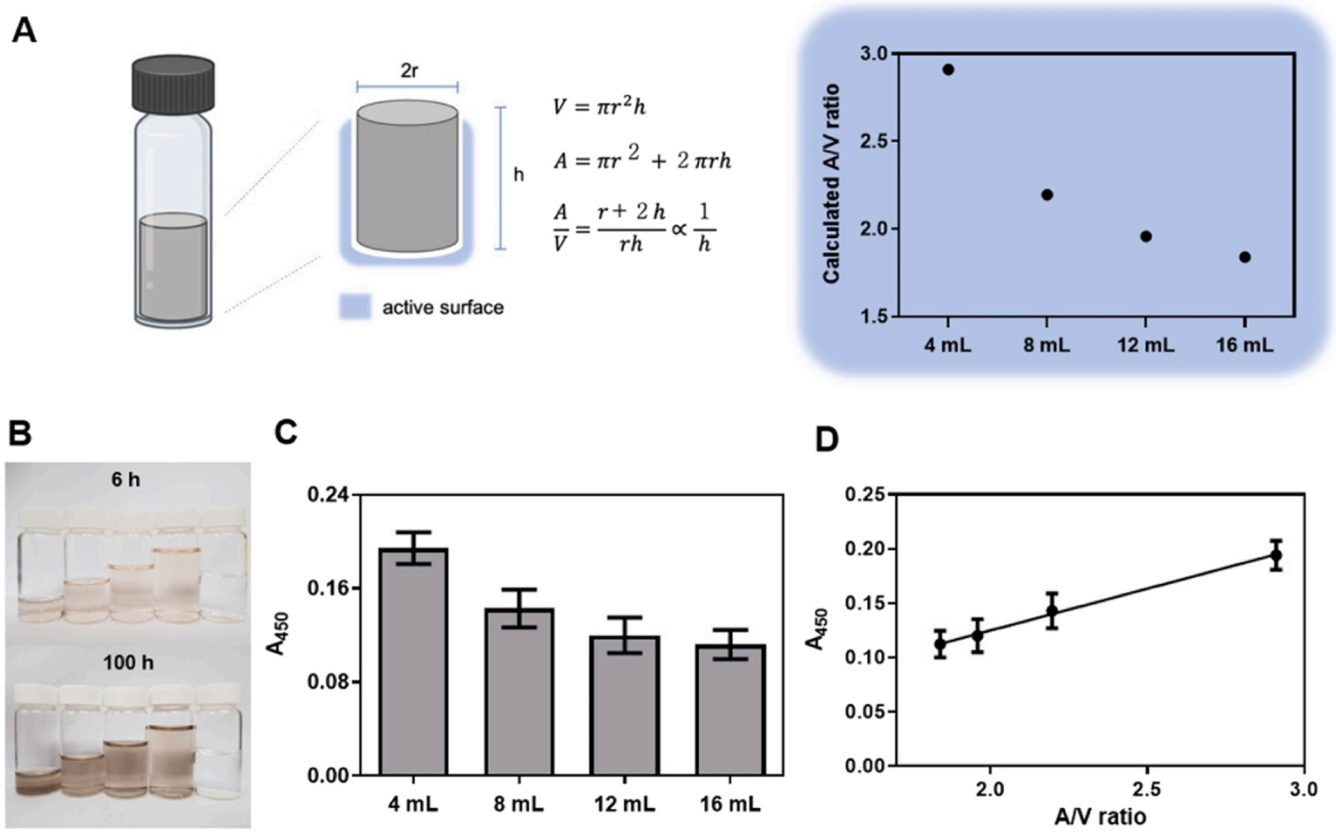

Fig. 1. (a) (left) The relationship between solution volume and its solid-liquid interface area in the current experimental system. (right) Calculated A/V ratios for different volumes of solutions. (b) Photographs of O_2 plasma-treated vials incubating different volumes (4 mL, 8 mL, 12 mL, and 16 mL) of solutions (2 mg/mL of dopamine) for 6 and 100 h. (c) Values of A_{450} measured from the solutions of (b) at 100 h. (d) A plot of A_{450} values against A/V ratios of each solution.

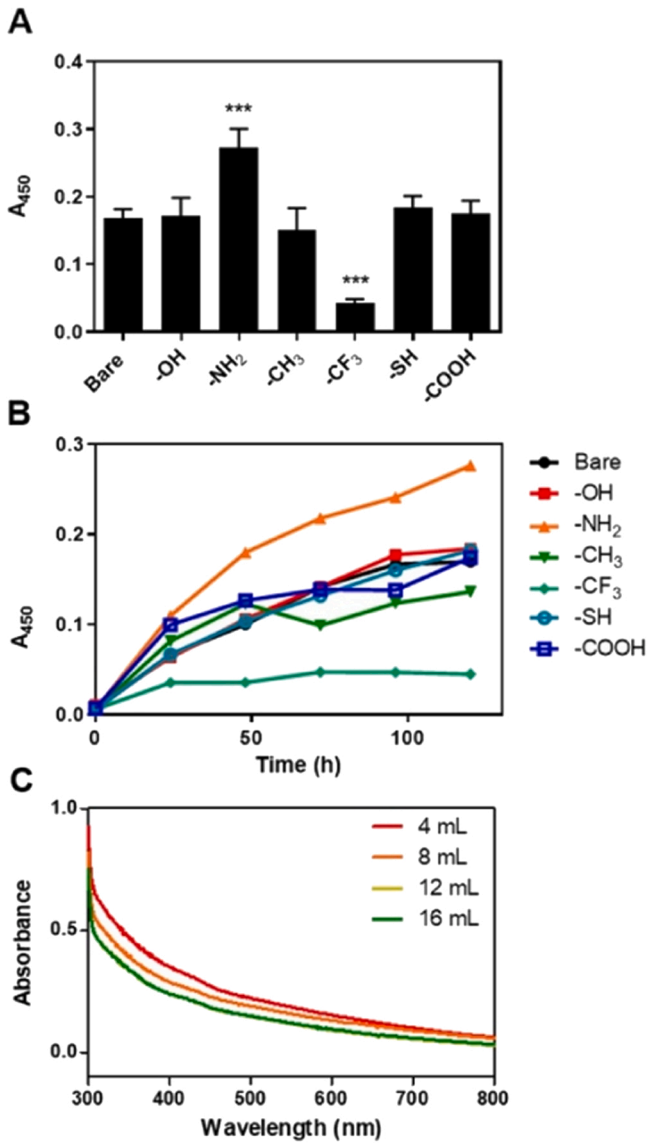

Fig. 2. (a,b) The influence of surface functional groups on the formation of pDA. The experiments were carried out in 4 mL of each solution (2 mg/mL of dopamine). (a) Averaged values of A_{450} at 120 h for each surface. The data were statistically analyzed by one-way analysis of variance (ANOVA). The points represent means ± s.d. (***$p < 0.001$). (b) Temporal changes of A_{450} for each surface. (c) UV–VIS absorbance spectra of solutions (2 mg/mL of dopamine) with different volumes at 120 h in vials modified with -NH_2 groups.

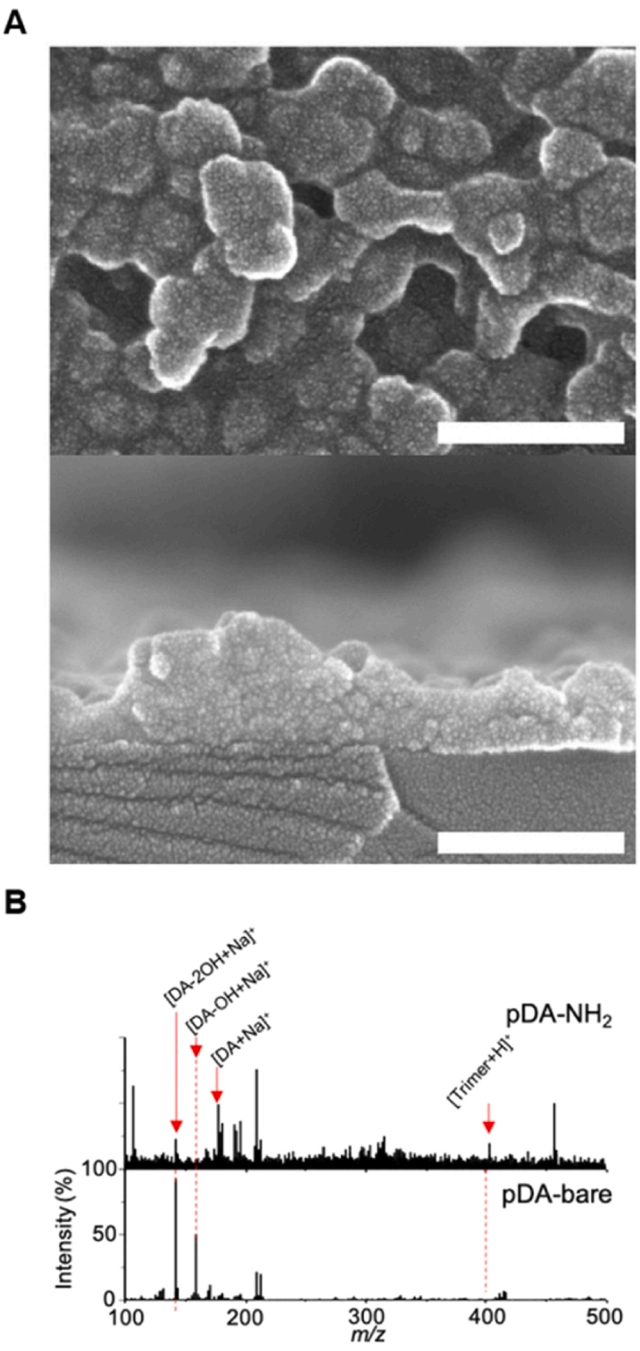

Fig. 3. (a) SEM images of solution-phase pDA synthesized with -NH_2 surface (top and side view, scale bars are 200 nm). (b) LDI-TOF-MS spectra of solution-dispersed phase of pDA synthesized with -NH_2 surfaces. The typical trimer peak was observed with the -NH_2 condition.

while being most remarkable at pH 7 (Fig. S6).

Having observed that the formation of solution-phase pDA may be regulated by functional groups at a solid-liquid interface, we next asked if it is chemically equivalent to conventionally synthesized pDA. We chose the -NH_2 surface for further analyses, as it was shown the most efficient in accelerating pDA formation. Dispersions of synthesized pDA were dried and the residual powders were analyzed using FE-SEM and LDI-TOF-MS. Fig. 3a shows the morphology of the solution-dispersed phase of pDA synthesized with an -NH_2 surface, showing spherical structures (with diameters of 60–70 nm) adhered to each other. Such morphological features of the pDA were comparable with previously reported pDA synthesized

by using an oxidant in an aqueous or a mixed solution. LDI-TOF-MS spectra of pDA synthesized with the –NH_2 surfaces presented a typical mass peak of pDA subunit at *m/z* 402 corresponding to a trimer of two DHIs and a pyrrolecarboxylic acid (Fig. 3b) [42]. In addition, there were two mass peaks at *m/z* 142 $[\text{dopamine - 2OH + Na}]^+$ and 177 $[\text{dopamine + Na}]^+$ which originated from fragmentation and sodiation of dopamine, respectively [43]. The results imply that the pDA synthesized with the –NH_2 surface has the characteristic substructures of conventional pDA along with physically intercalated dopamine monomers. By contrast, the typical mass peak of pDA subunit was not detected from pDA synthesized with the bare surface, while the mass peak at *m/z* 142 $[\text{dopamine - 2OH + Na}]^+$ was intensified with appearance of a new peak at *m/z* 159 $[\text{dopamine - OH + Na}]^+$. This indicates the pDA synthesized with the bare

surface was mainly composed of monomeric dopamine with a much lower degree of polymerization than the pDA synthesized with the –NH_2

surface. LDI-TOF-MS analyses further confirm that the -NH_2 functional groups on the surface of a glass vial promote polymerization of dopamine. Collectively, the data in Fig. 3 suggests that the surface modified with -NH_2 groups accelerates pDA formation, not much altering its morphological features and molecular components.

For decades, pDA has attracted interest from various fields for its ability to form a thin film compatible with further covalent functionalization in a substrate type-independent manner [9]. An interesting aspect of pDA film is that it generally requires a moderately basic pH and amine-containing molecules in solution, except occasions using highly oxidizing and extreme hydrothermal conditions [44,45]. Lee et al. have suggested that the amine molecules may work as a crosslinker connecting oxidized dopamine derivatives via bivalent cation-π interactions [46]. The mechanism of film deposition depends on a sedimentation-like process of oligomeric molecular complexes, which makes amine moieties (or other molecules that enable the crosslinking) crucial in the formation of pDA films. Amines that are immobilized on surface, on the other hand, are expected to be less effective in crosslinking aromatic intermediates, and thus less so in promoting the deposition of pDA films. To characterize the film-phase of pDA, we prepared -NH_2-modified Si wafers and analyzed them after incubating in an aqueous solution (pH 7) of dopamine. Albeit low pH and the absence of amine-containing molecules in solution, a very thin film was deposited onto the surfaces, which we could identify by observing a slight color change (Fig. 4a) and conducting ellipsometric measurements. The

films became gradually rougher, thicker, and hydrophilic (Fig. 4b). However, the changes were minute, indicating that the deposition occurred at the very initial period and did not proceed significantly afterwards. This was opposed to the case of solution-phase amines, which led to the deposition of much thicker multi-layered films. To examine detailed morphological features of the surfaces, we conducted AFM analysis. As shown in Fig. 4c, spherical pDA species with diameters of 10–20 nm were observed on both surfaces, with their numbers increasing for longer incubation. The pDA species adhered to the surfaces often (but not always) existed as groups in size of approximately 200–300 nm, indicating the presence of attractive interactions between themselves. The results on the surfaces collectively suggest that pDA species primarily formed near the surfaces and are subsequently detached into the solution without multilayer-deposition.

We next set out to ask if surfaces of amyloid fibers would be similarly active to those of vials in regulating pDA formation. We slightly modified a short peptide recently reported to spontaneously self-assemble (Ac-IHIHIXI-NH_2; X = Y or Q) [47] by replacing His with Lys. This heptapeptide system is a useful platform to study chemical properties of amyloid fibers, as it protrudes the polar residues outside and buries the nonpolar residues within itself in its amyloid form (Fig. 5a). The Lys residues in our sequence (Ac-IKIKIYI-NH_2; IKY) are, thus, expected to be periodically presented on the surface of the amyloid fibers, which gives a chemical environment similar to the surface of an amine-modified vial. As expected, the presence of IKY fibers (Figs. 5b and S7) facilitated pDA formation. The amount of pDA formed with the fibers was almost 2.5 fold higher than that without after 120 h of incubation (Fig. 5c). When Lys was replaced with His (Ac-IHIHIYI-NH_2; IHY), the influence became weaker, indicating surface-enriched amine moieties are superior to simple positive charges in accelerating pDA formation (Figs. 5c and S8). In addition, IKY or IHY fibers led to changes in morphology and water-dispersibility of pDA. Inclusion of fibers in pDA resulted in larger aggregates that dispersed much better in an aqueous solution than in the case without (Fig. 5d), which is consistent with our previous results with amyloid fibers of various proteins [37]. Overall, the data with IKY fibers support that amine moieties located on surfaces of amyloid fibers play a decisive role in regulating pDA formation, as we observed in amine-modified vial surfaces.

4. Discussions

The analytic results of the solution-dispersed and surface-coated phases of pDA show that the roles of amine moieties may depend drastically on where they are located (i.e., those in solution and at surface). Amines in solution can participate into pDA and crosslink its oligomeric structures via cation-π interactions, altering their morphological and paramagnetic properties [48]. Amines at solid-liquid interfaces, on the other hand, are likely unable to do so. They would rather covalently capture oxidized products of dopamine, increasing their local effective concentrations. Reflecting this difference, amines immobilized on solid-liquid interfaces led to the formation of extremely thin pDA films, leaving the majority of pDA as dispersions in the solution. This is opposed to the deposition of thick films in previously reported cases using an amine-containing buffer at basic pHs [49–51]. Interestingly, the immobilized amines were rather functional for accelerating the formation of solution-dispersed pDA formation. Influences of the chemical structure of the substrate on the formation of pDA films

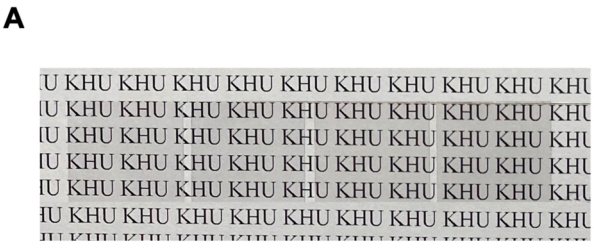

	24 h	72 h	96 h	120 h
Rq (nm)	3.082	5.678	4.975	7.527
Thickness (nm)	5.21 ± 1.28	6.115 ± 0.26	7.4 ± 0.28	7.115 ± 0.83
WCA (degree)	54.39	43.9	47.97	42.29

Fig. 4. (a) Photos of -NH_2-derivatized coverslips incubated in a dopamine solution (4 mL, 2 mg/mL) for 0, 24, 96, and 120 h (from the left to the right). (b) Measured values of roughness, thickness, and water contact angles (WCA) of the -NH_2 modified surfaces. (c) AFM images of -NH_2 surfaces incubated in the dopamine solution.

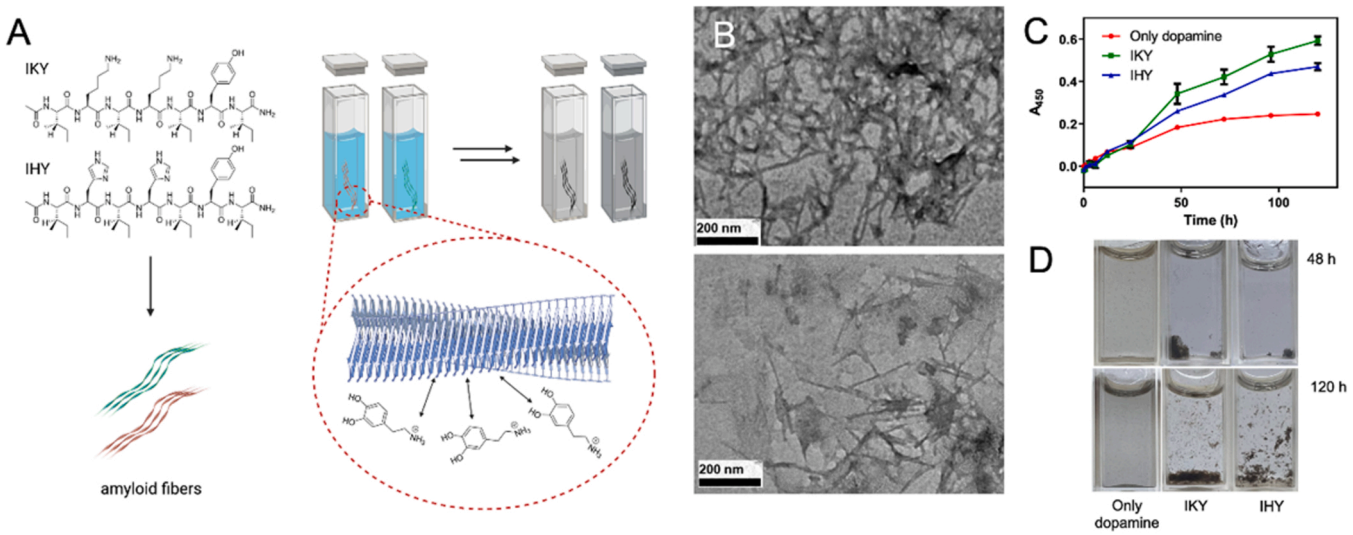

Fig. 5. (a) Schematic description of the experiment with amyloid fibers. (b) TEM images of amyloid fibers (top: IKY, bottom: IHY). (c) A_{450} of pDA synthesized with short-peptide-based amyloids. Background absorbance of amyloid fiber is corrected. (d) Photos of solutions with and without each amyloid fiber incubated with dopamine (2 mg/mL) for desired times.

thereon have recently started to be examined by spectroscopic methods [52–54]. The mussel-inspired pDA films are chemically similar to natural melanins, but have characteristics not compatible with intracellular environment, such as nonspecific adhesiveness toward solid surfaces and uncontrollable formation kinetics. Amyloid scaffolds of Pmel17 provide a plenty of lysines—along with other polar residues—displayed on their surface, which are expected to have critical influences on the kinetic and materials properties of biosynthesized melanins.

5. Conclusions

In summary, we showed that the formation of solution-dispersed pDA was facilitated by functional groups at solid-liquid interfaces, and the identity of the functional group determined the strength of such an influence. Amine-functionalized surfaces were most effective in the facilitating function, whereas non-polar moieties were measured to be less so. Further analyses of pDA formed with the NH_2 surfaces indicated that pDA mainly formed as a solution-dispersed form along with nanometers-thick films, and their general properties were similar to conventional pDA species. Amyloid fibers capable of displaying lysines and histidines on their surface were used to show that the spatially oriented functional groups were particularly active in facilitating the pDA formation similarly to those immobilized on the vial surfaces. This study gives implications on the currently unappreciated roles of functional amyloid scaffolds in melanogenesis, and general supramolecular functionality manifested by locally enriching functional groups at solid-liquid interfaces. Apart from biochemical implications, this study reveals an unprecedented surface-dependent mechanism of pDA formation, providing practically useful information in setting up experimental schemes for pDA synthesis.

CRediT authorship contribution statement

Chan Yeon Kim: Methodology, Data curation, Formal analysis, Investigation, Writing – original draft. **Yoonyoung Kim:** Methodology, Data curation, Formal analysis. **Min Young Lee:** Methodology, Validation, Investigation, Resources. **Seong Ah Jo:** Methodology, Validation, Investigation, Resources. **Seung-Woo Kim:** Validation, Investigation. **Sung Min Kang**: Formal analysis, Writing - review & editing. **Young-Kwan Kim:** Supervision, Writing – review & editing. **Kyungtae Kang:** Conceptualization, Project administration, Supervision, Funding acquisition, Writing – review & editing.

Declaration of Competing Interest

The authors declare that they have no known competing financial interests or personal relationships that could have appeared to influence the work reported in this paper.

Data availability

Data will be made available on request.

Acknowledgments

This work was supported by the National Research Foundation of Korea (NRF) grant funded by the Ministry of Science, ICT & Future Planning (MSIP) (2019R1C1C1009111), and the GRRC Program of Gyeonggi Province [GRRC-kyunghee2017(A01)]. This work was also supported by the Commercialization Promotion Agency for R&D Outcomes (COMPA) funded by the Ministry of Science and ICT (MSIT) (2022-URE-04, quantitative detection of low molecular weight compounds by using laser desorption/ionization mass spectrometry).

Appendix A. Supplementary material

Supplementary data associated with this article can be found in the online version at doi:10.1016/j.colsurfb.2022.113068.

References

[1] M. d'Ischia, K. Wakamatsu, A. Napolitano, S. Briganti, J.C. Garcia-Borron, D. Kovacs, P. Meredith, A. Pezzella, M. Picardo, T. Sarna, J.D. Simon, S. Ito, Melanins and melanogenesis: methods, standards, protocols, Pigment Cell Melanoma Res. 26 (2013) 616–633, https://doi.org/10.1111/pcmr.12121.
[2] M. d'Ischia, K. Wakamatsu, F. Cicoira, E. Di Mauro, J.C. Garcia-Borron, S. Commo, I. Galvan, G. Ghanem, K. Kenzo, P. Meredith, A. Pezzella, C. Santato, T. Sarna, J. D. Simon, L. Zecca, F.A. Zucca, A. Napolitano, S. Ito, Melanins and melanogenesis: from pigment cells to human health and technological applications, Pigment Cell Melanoma Res. 28 (2015) 520–544, https://doi.org/10.1111/pcmr.12393.
[3] K.J. McGraw, An update on the honesty of melanin-based color signals in birds, Pigment Cell Melanoma Res. 21 (2008) 133–138, https://doi.org/10.1111/j.1755-148X.2008.00454.x.
[4] C.D. Derby, Cephalopod Ink: production, chemistry, functions and applications, Mar. Drugs 12 (2014) 2700–2730, https://doi.org/10.3390/md12052700.
[5] P. Karlson, C.E. Sekeris, N-Acetyl-dopamine as sclerotizing agent of the insect cuticle, Nature 195 (1962) 183–184, https://doi.org/10.1038/195183a0.

[6] H.C. Eisenman, A. Casadevall, Synthesis and assembly of fungal melanin, Appl. Microbiol. Biotechnol. 93 (2012) 931–940, https://doi.org/10.1007/s00253-011-3777-2.

[7] N. Gessler, A. Egorova, T. Belozerskaya, Melanin pigments of fungi under extreme environmental conditions (Review), Appl. Microbiol. Biotechnol. 50 (2014) 105–113, https://doi.org/10.1134/S0003683814020094.

[8] M.E. Pavan, N.I. López, M.J. Pettinari, Melanin biosynthesis in bacteria, regulation and production perspectives, Appl. Microbiol. Biotechnol. 104 (2020) 1357–1370, https://doi.org/10.1007/s00253-019-10245-y.

[9] J.H. Ryu, P.B. Messersmith, H. Lee, Polydopamine surface chemistry: a decade of discovery, ACS Appl. Mater. Interfaces 10 (2018) 7523–7540, https://doi.org/10.1021/acsami.7b19865.

[10] T.G. Barclay, H.M. Hegab, S.R. Clarke, M. Ginic-Markovic, Versatile surface modification using polydopamine and related polycatecholamines: chemistry, structure, and applications, Adv. Mater. Interfaces 4 (2017), 1601192, https://doi.org/10.1002/admi.201601192.

[11] H. Lee, S.M. Dellatore, W.M. Miller, P.B. Messersmith, Mussel-inspired surface chemistry for multifunctional coatings, Science 318 (2007) 426–430, https://doi.org/10.1126/science.1147241.

[12] Y. Liu, K. Ai, J. Liu, M. Deng, Y. He, L. Lu, Dopamine-melanin colloidal nanospheres: an efficient near-infrared photothermal therapeutic agent for in vivo cancer therapy, Adv. Mater. 25 (2013) 1353–1359, https://doi.org/10.1002/adma.201204683.

[13] P. Yang, S. Zhang, N. Zhang, Y. Wang, J. Zhong, X. Sun, Y. Qi, X. Chen, Z. Li, Y. Li, Tailoring synthetic melanin nanoparticles for enhanced photothermal therapy, ACS Appl. Mater. Interfaces 11 (2019) 42671–42679, https://doi.org/10.1021/acsami.9b16861.

[14] X. Wang, J. Zhang, Y. Wang, C. Wang, J. Xiao, Q. Zhang, Y. Cheng, Multi-responsive photothermal-chemotherapy with drug-loaded melanin-like nanoparticles for synergetic tumor ablation, Biomaterials 81 (2016) 114–124, https://doi.org/10.1016/j.biomaterials.2015.11.037.

[15] W. Lei, K. Ren, T. Chen, X. Chen, B. Li, H. Chang, J. Ji, Polydopamine nanocoating for effective photothermal killing of bacteria and fungus upon near-infrared irradiation, Adv. Mater. Interfaces (2016), 1600767, https://doi.org/10.1002/admi.201600767.

[16] M.H. Ryou, Y.M. Lee, J.K. Park, J.W. Choi, Mussel-inspired polydopamine-treated polyethylene separators for high-power Li-ion batteries, Adv. Mater. 23 (2011) 3066–3070, https://doi.org/10.1002/adma.201100303.

[17] T. Sun, Z.-J. Li, H.-G. Wang, D. Bao, F.-L. Meng, X.-B. Zhang, A biodegradable polydopamine-derived electrode material for high-capacity and long-life lithium-ion and sodium-ion batteries, Angew. Chem. Int. Ed. 55 (2016) 10662–10666, https://doi.org/10.1002/anie.201604519.

[18] K. Qu, Y. Zheng, Y. Jiao, X. Zhang, S. Dai, S.Z. Qiao, Polydopamine-inspired, dual heteroatom-doped carbon nanotubes for highly efficient overall eater splitting, Adv. Energy Mater. 7 (2017), 1602068, https://doi.org/10.1002/aenm.201602068.

[19] H.J. Nam, B. Kim, M.J. Ko, M. Jin, J.M. Kim, D.Y. Jung, A new mussel-inspired polydopamine sensitizer for dye-sensitized solar cells: controlled synthesis and charge transfer, Chem. Eur. J. 18 (2012) 14000–14007, https://doi.org/10.1002/chem.201202283.

[20] N. Ahmad, X. Zhang, S. Yang, D. Zhang, J. Wang, S. uz Zafar, Y. Li, Y. Zhang, S. Hussain, Z. Cheng, Polydopamine/ZnO electron transport layers enhance charge extraction in inverted non-fullerene organic solar cells, J. Mater. Chem. C 7 (2019) 10795–10801, https://doi.org/10.1039/C9TC02781E.

[21] Z.E. Siwicka, F.A. Son, C. Battistella, M.H. Moore, J. Korpanty, N.C. McCallum, Z. Wang, B.J. Johnson, O.K. Farha, N.C. Gianneschi, Synthetic porous melanin, J. Am. Chem. Soc. 143 (2021) 3094–3103, https://doi.org/10.1021/jacs.0c10465.

[22] X. Zhou, N.C. McCallum, Z. Hu, W. Cao, K. Gnanasekaran, Y. Feng, J.F. Stoddart, Z. Wang, N.C. Gianneschi, Artificial allomelanin nanoparticles, ACS Nano 13 (2019) 10980–10990, https://doi.org/10.1021/acsnano.9b02160.

[23] N.C. McCallum, F.A. Son, T.D. Clemons, S.J. Weigand, K. Gnanasekaran, C. Battistella, B.E. Barnes, H. Abeyratne-Perera, Z.E. Siwicka, C.J. Forman, X. Zhou, M.H. Moore, D.A. Savin, S.I. Stupp, Z. Wang, G.J. Vora, B.J. Johnson, O.K. Farha, N.C. Gianneschi, Allomelanin: a biopolymer of intrinsic microporosity, J. Am. Chem. Soc. 143 (2021) 4005–4016, https://doi.org/10.1021/jacs.1c00748.

[24] V. Ball, Polydopamine films and particles with catalytic activity, Catal. Today 301 (2018) 196–203, https://doi.org/10.1016/j.cattod.2017.01.031.

[25] M. Kang, E. Kim, Z. Temoçin, J. Li, E. Dadachova, Z. Wang, L. Panzella, A. Napolitano, W.E. Bentley, G.F. Payne, Reverse engineering to characterize redox properties: revealing melanin's redox activity through mediated electrochemical probing, Chem. Mater. 30 (2018) 5814–5826, https://doi.org/10.1021/acs.chemmater.8b02428.

[26] V. Capozzi, G. Perna, P. Carmone, A. Gallone, M. Lastella, E. Mezzenga, G. Quartucci, M. Ambrico, V. Augelli, P.F. Biagi, T. Ligonzo, A. Minafra, L. Schiavulli, M. Pallara, R. Cicero, Optical and photoelectronic properties of melanin, Thin Solid Films 511 (2006) 362–366, https://doi.org/10.1016/j.tsf.2005.12.065.

[27] M.G. Bridelli, P.R. Crippa, Infrared and water sorption studies of the hydration structure and mechanism in natural and synthetic melanin, J. Phys. Chem. B 114 (2010) 9381–9390, https://doi.org/10.1021/jp101833k.

[28] L. Panzella, G. Gentile, G. D'Errico, N.F. Della Vecchia, M.E. Errico, A. Napolitano, C. Carfagna, M. d'Ischia, Atypical structural and π-electron features of a melanin polymer that lead to superior free-radical-scavenging properties, Angew. Chem. Int. Ed. 52 (2013) 12684–12687, https://doi.org/10.1002/anie.201305747.

[29] A. Corani, A. Huijser, T. Gustavsson, D. Markovitsi, P.A. Malmqvist, A. Pezzella, M. d'Ischia, V. Sundstrom, Superior photoprotective motifs and mechanisms in eumelanins uncovered, J. Am. Chem. Soc. 136 (2014) 11626–11635, https://doi.org/10.1021/ja501499q.

[30] M. d'Ischia, A. Napolitano, A. Pezzella, P. Meredith, M. Buehler, Melanin biopolymers: tailoring chemical complexity for materials design, Angew. Chem. Int. Ed. 59 (2020) 11196–11205, https://doi.org/10.1002/anie.201914276.

[31] D.M. Fowler, A.V. Koulov, C. Alory-Jost, M.S. Marks, W.E. Balch, J.W. Kelly, Functional amyloid formation within mammalian tissue, PLoS Biol. 4 (2006), e6, https://doi.org/10.1371/journal.pbio.0040006.

[32] R.P. McGlinchey, F. Shewmaker, P. McPhie, B. Monterroso, K. Thurber, R.B. Wickner, The repeat domain of the melanosome fibril protein Pmel17 forms the amyloid core promoting melanin synthesis, Proc. Natl. Acad. Sci. USA, 106, 2009, pp. 13731–13736. ⟨http://doi.org/10.1073/pnas.0906509106⟩.

[33] J.F. Berson, D.C. Harper, D. Tenza, G. Raposo, M.S. Marks, Pmel17 initiates premelanosome morphogenesis within multivesicular bodies, Mol. Biol. Cell 12 (2001) 3451–3464, https://doi.org/10.1091/mbc.12.11.3451.

[34] A.C. Theos, S.T. Truschel, G. Raposo, M.S. Marks, The silver locus product Pmel17/gp100/Silv/ME20: controversial in name and in function, Pigment Cell Res. 18 (2005) 322–336, https://doi.org/10.1111/j.1600-0749.2005.00269.x.

[35] R.M. Leonhardt, N. Vigneron, C. Rahner, P. Cresswell, Proprotein convertases process pmel17 during secretion, J. Biol. Chem. 286 (2011) 9321–9337, https://doi.org/10.1074/jbc.M110.168088.

[36] J.C. Valencia, T. Hoashi, J.M. Pawelek, F. Solano, V.J. Hearing, Pmel17: controversial indeed but critical to melanocyte function, Pigment Cell Res. 19 (2006) 250–252, https://doi.org/10.1111/j.1600-0749.2006.00308.x.

[37] J. Shin, N.T.K. Le, H. Jang, T. Lee, K. Kang, Supramolecular regulation of polydopamine formation by amyloid fibers, Chem. Eur. J. 26 (2020) 5500–5507, https://doi.org/10.1002/chem.202000437.

[38] H. Park, H. Jeon, M.Y. Lee, H. Jeon, S. Kwon, S. Hong, K. Kang, Designed amyloid fibers with emergent melanosomal functions, Langmuir 38 (2022) 7077–7084, https://doi.org/10.1021/acs.langmuir.2c00904.

[39] D. Ha, K. Kang, Nucleophilic regulation of the formation of melanin-like species by amyloid fibers, ACS Omega 7 (2021) 773–779, https://doi.org/10.1021/acsomega.1c05399.

[40] D. Li, E.M. Jones, M.R. Sawaya, H. Furukawa, F. Luo, M. Ivanova, S.A. Sievers, W. Wang, O.M. Yaghi, C. Liu, D.S. Eisenberg, Structure-based design of functional amyloid materials, J. Am. Chem. Soc. 136 (2014) 18044–18051, https://doi.org/10.1021/ja509648u.

[41] H.A. Lee, Y.F. Ma, F. Zhou, S. Hong, H. Lee, Material-independent surface chemistry beyond polydopamine coating, Acc. Chem. Res. 52 (2019) 704–713, https://doi.org/10.1021/acs.accounts.8b00583.

[42] Q. Lyu, N. Hsueh, C.L.L. Chai, Unravelling the polydopamine mystery: is the end in sight, Polym. Chem. 10 (2019) 5771–5777, https://doi.org/10.1039/C9PY01372E.

[43] Y.-K. Kim, R. Landis, R.W. Vachet, V.M. Rotello, Matrix-incorporated polydopamine layer as a simple, efficient, and universal coating for laser desorption/ionization time-of-flight mass spectrometric analysis, ACS Appl. Mater. Interfaces 10 (2018) 36361–36368, https://doi.org/10.1021/acsami.8b10990.

[44] F. Ponzio, J. Barthes, J. Bour, M. Michel, P. Bertani, J. Hemmerle, M. d'Ischia, V. Ball, Oxidant control of polydopamine surface chemistry in acids: a mechanism-based entry to superhydrophilic-superoleophobic coatings, Chem. Mater. 28 (2016) 4697–4705, https://doi.org/10.1021/acs.chemmater.6b01587.

[45] W. Zheng, H. Fan, L. Wang, Z. Jin, Oxidative self-polymerization of fopamine in an acidic environment, Langmuir 31 (2015) 11671–11677, https://doi.org/10.1021/acs.langmuir.5b02757.

[46] S. Hong, Y. Wang, S.Y. Park, H. Lee, Progressive fuzzy cation-π assembly of biological catecholamines, Sci. Adv. 4 (2018) eaat7457, https://doi.org/10.1126/sciadv.aat7457.

[47] C.M. Rufo, Y.S. Moroz, O.V. Moroz, J. Stöhr, T.A. Smith, X. Hu, W.F. DeGrado, I. V. Korendovych, Short peptides self-assemble to produce catalytic amyloids, Nat. Chem. 6 (2014) 303–309, https://doi.org/10.1038/nchem.1894.

[48] N.F.D. Vecchia, A. Luchini, A. Napolitano, G. D'Errico, G. Vitiello, N. Szekely, M. d'Ischia, L. Paduano, Tris buffer modulates polydopamine growth, aggregation, and paramagnetic properties, Langmuir 30 (2014) 9811–9818.

[49] F. Bernsmann, A. Ponche, C. Ringwald, J. Hemmerlé, J. Raya, B. Bechinger, J.-C. Voegel, P. Schaaf, V. Ball, Characterization of dopamine−melanin growth on silicon oxide, J. Phys. Chem. C 113 (2009) 8234–8242, https://doi.org/10.1021/jp901188h.

[50] H. Lee, S.M. Dellatore, W.M. Miller, P.B. Messersmith, Mussel-inspired surface chemistry for multifunctional coatings, Science 318 (2007) 426–430, https://doi.org/10.1126/science.1147241.

[51] O. Pop-Georgievski, Š. Popelka, M. Houska, D. Chvostová, V. Proks, F. Rypáček, Poly(ethylene oxide) layers grafted to dopamine-melanin anchoring layer: stability and resistance to protein adsorption, Biomacromolecules 12 (2011) 3232–3242, https://doi.org/10.1021/bm2007086.

[52] G. Sun, F. Zu, N. Koch, J. Rappich, K. Hinrichs, In situ infrared spectroscopic monitoring and characterization of the growth of polydopamine (PDA) films, Phys. Status Solidi B 256 (2019), 1800308, https://doi.org/10.1002/pssb.201800308.

[53] J. Svoboda, M. Král, M. Dendisová, P. Matějka, O. Pop-Georgievski, Colloids Surf. B, 205, 2021, 11897. ⟨https://doi.org/10.1016/j.colsurfb.2021.111897⟩.

[54] M. Král, M. Dendisová, P. Matějka, J. Svoboda, O. Pop-Georgievski, Colloids Surf. B, 221, 2023, 112954. ⟨https://doi.org/10.1016/j.colsurfb.2022.112954⟩.